

Development, importance, and effect of a ground truth correction for the Moon Mineralogy Mapper reflectance data set

Peter J. Isaacson,¹ Noah E. Petro,² Carle M. Pieters,³ Sebastien Besse,⁴ Joseph W. Boardman,⁵ Roger N. Clark,⁶ Robert O. Green,⁷ Sarah Lundeen,⁷ Erick Malaret,⁸ Stephanie McLaughlin,⁴ Jessica M. Sunshine,⁴ and Lawrence A. Taylor⁹

Received 4 January 2012; revised 19 December 2012; accepted 21 December 2012; published 7 March 2013.

[1] We evaluate the effect and importance of a ground truth correction for the Moon Mineralogy Mapper (M³) level 2 (reflectance) data set. This correction is derived from extensive laboratory characterizations of mature feldspathic lunar soils and is designed to improve the accuracy of 1 μm absorption features in M³ reflectance data. To evaluate the correction, the band strength across a subset of the feldspathic highlands terrane (FHT) is analyzed with M³ imaging spectroscopy data. Using M³ reflectance data and derived products, we find significant differences in band strength and shape between M³ observations collected over identical terrain but under different observational and operational conditions. The ground truth correction minimizes these differences in 1 μm band strengths and also brings the 1 μm band strengths measured with M³ data into closer agreement with laboratory measurements of lunar soil samples. Although the FHT region studied was found to have very low band strengths, the M³ ground truth correction results in overall stronger absorption features for all mature soils relative to uncorrected level 2 (reflectance) data for the same region. These differences between M³ data collected under different operational conditions and the effects of the ground truth correction, while minor in appearance, can have significant implications for interpretations of any regional soil analyses with M³ data that rely on absolute 1 μm absorption feature strength. The M³ ground truth correction corrects only wavelengths below ~ 1500 nm, and comparisons between corrected and uncorrected wavelengths must be done with caution.

Citation: Isaacson, P. J., et al. (2013), Development, importance, and effect of a ground truth correction for the Moon Mineralogy Mapper reflectance data set, *J. Geophys. Res. Planets*, 118, 369–381, doi:10.1002/jgre.20048.

1. Introduction

1.1. Origin and Significance of 1 μm Features in Lunar Spectroscopy

[2] Visible to near-infrared reflectance spectra of common lunar minerals exhibit absorption features near 1 μm . These

features are caused by ferrous iron (Fe²⁺) in mineral lattice sites [e.g., Burns, 1993]. In remote observations of the lunar surface, the strength of the 1 μm feature is controlled by a range of properties of the surface, including mineralogy (relative mineral abundance), mineral composition, grain size, and degree of space weathering, among others [e.g., Adams, 1974; Clark, 1995; Cloutis and Gaffey, 1991; Hapke, 2001; Hazen et al., 1978; Hiroi and Pieters, 1994; Isaacson et al., 2011a; Klima et al., 2007; Mustard and Pieters, 1987; Noble et al., 2001; Pieters et al., 2000; Poulet and Erard, 2004; Sunshine and Pieters, 1998]. The 1 μm absorption feature is one of the primary means for evaluating mineralogy with visible to near-infrared observations of the lunar surface.

[3] The goal of this investigation is to discuss the development of, rationale for, quantification of, and evaluation of a ground truth correction for the M³ data set. This is accomplished through an analysis of the absolute strength of the 1 μm ferrous absorption feature in the feldspathic highlands terrane (FHT) defined by Jolliff et al. [2000], over a region where M³ data were collected under two substantially different operational conditions (high Sun angle, high signal levels, warm detector and low Sun angle, low signal levels, and cold detector; for details on M³ operational conditions and history, see Boardman et al. [2011] and Green et al. [2011]). Previous

All Supporting Information may be found in the online version of this article.

¹Hawaii Institute of Geophysics and Planetology, School of Ocean and Earth Science and Technology, University of Hawaii at Mānoa, Honolulu, Hawaii, USA.

²NASA/Goddard Space Flight Center, Greenbelt, Maryland, USA.

³Department of Geological Sciences, Brown University, Providence, Rhode Island, USA.

⁴Astronomy Department, University of Maryland, College Park, Maryland, USA.

⁵Analytical Imaging Geophysics, Boulder, Colorado, USA.

⁶United States Geological Survey, Denver, Colorado, USA.

⁷Jet Propulsion Laboratory, Pasadena, California, USA.

⁸Applied Coherent Technology, Herndon, Virginia, USA.

⁹Planetary Geosciences Institute, University of Tennessee, Knoxville, Tennessee, USA.

Corresponding author: P. J. Isaacson, Hawaii Institute of Geophysics and Planetology, School of Ocean and Earth Science and Technology, University of Hawaii at Manoa, Honolulu, HI 96822, USA. (isaacson@higp.hawaii.edu)

©2013. American Geophysical Union. All Rights Reserved.
2169-9097/13/10.1002/jgre.20048

analyses indicate that the FHT is relatively homogenous and feldspathic in composition [e.g., *Jolliff et al.*, 2000], meaning that it should exhibit relatively weak but constant 1 μm bands. Thus, it is an appropriate region in which to assess M³ data collected under the range of conditions M³ experienced throughout the mission and to characterize the magnitude of absorption features observed in M³ data.

1.2. M³ and Chandrayaan-1

1.2.1. M³ and Chandrayaan-1 Overview

[4] M³ is a pushbroom imaging spectrometer that flew on the Chandrayaan-1 mission, the first lunar mission of the Indian Space Research Organisation (ISRO). M³ collected high spatial and spectral resolution data across visible to near-infrared wavelengths (~ 400 to ~ 3000 nm), meeting its requirement to acquire data over at least 90% of the lunar surface. M³ acquired data in imaging mode, meaning that for every image pixel, a contiguous spectrum of data covering the full wavelength range was measured. Additional details on the Chandrayaan-1 mission are provided by *Goswami and Annadurai* [2009], and more details on the M³ instrument design and measurement strategy are provided by *Mouroulis et al.* [2007], *Pieters et al.* [2009], *Rodriguez et al.* [2009], *Green et al.* [2011], and *Boardman et al.* [2011]. Chandrayaan-1 was intended to orbit the Moon for a 2 year nominal mission in a 100 km polar orbit, allowing for full coverage of the Moon by a number of optical instruments on Chandrayaan-1, and enabling M³ to cover the Moon several times over a range of viewing geometries.

1.2.2. Spacecraft Thermal Challenges

[5] Early in the Chandrayaan-1 mission, operational challenges were encountered. The Chandrayaan-1 spacecraft was plagued by thermal problems resulting from the intense thermal environment in the 100 km lunar polar orbit. These issues led to M³ being operated well outside its intended detector temperature range (156 ± 3 K) for much of the mission, which led to substantial challenges related to calibration of the collected data [*Green et al.*, 2011; *Rodriguez et al.*, 2009]. The operational conditions experienced by M³ are illustrated in Figure 1, which plots the detector temperature and beta angle (defined as the angle between the orbit plane and the solar vector; low beta angles indicate the high Sun conditions desired for imaging spectrometers like M³) for each M³ image. M³ files are numbered sequentially, so M³ file numbers do not directly indicate time, but are in order of acquisition [*Green et al.*, 2011]. As illustrated by Figure 1, M³ was operated outside of its intended operational conditions for nearly the entire mission.

[6] The operational conditions and their effect on the temperature of the M³ detector were closely correlated with viewing geometry: higher Sun angles led to a more intense thermal radiation environment, a warmer spacecraft, and thus a warmer M³ detector. In general, a higher detector temperature led to more “noisy” M³ data, although the noise level could not be sufficiently quantified as laboratory calibration data were not acquired for the extreme (both warm and cold) conditions experienced by M³ over the course of the mission. The noisy data collected with a warm detector were mitigated somewhat by the higher signal levels obtained during this period, because the warm detector conditions generally occurred during periods of high Sun (see

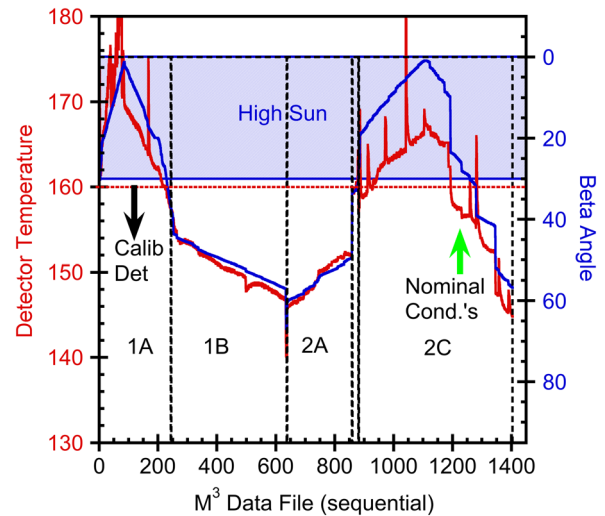


Figure 1. Illustration of the operational conditions experienced for each data file acquired by M³ over the course of the Chandrayaan-1 mission, modified from *Green et al.* [2011]. The red line is the M³ detector temperature (left axis), and the blue line is beta angle (right axis). M³ was designed to operate with a relatively cold detector (156 ± 3 K) and at low beta angle ($< 30^\circ$, high Sun). Over nearly the entire mission, M³ was operated well outside these conditions; the arrow near file number 1200 indicates the period of the mission when M³ was operated under “nominal” conditions. The horizontal line at 160 K indicates the M³ target maximum operation temperature; data collected with detector temperatures exceeding this value were calibrated through a combination of extrapolation and image-based approaches.

Figure 1). The unanticipated thermal conditions forced the Chandrayaan-1 mission operations team to operate the spacecraft’s science payload (including M³) only during periods of lower Sun angles during early parts of the mission. During this period, the temperature of the M³ detector was relatively low and thus the acquired data had relatively low noise levels, but the low Sun angles also led to correspondingly low signal levels. Later in the mission, the Chandrayaan-1 mission operations team elected to raise the spacecraft’s orbit altitude to 200 km, which provided a less intense thermal environment for the spacecraft and science payloads. During this period (defined as “optical period 2C” by the M³ team [*Boardman et al.*, 2011]), M³ acquired data over a range of detector temperatures, ranging from quite warm (> 160 K) to quite cold (< 150 K); the temperatures were closely linked to viewing geometry, as discussed above. On the whole, M³ acquired data over a wide range of thermal conditions, much of it well outside of the nominal range for which reliable ground calibration data were acquired [*Green et al.*, 2011].

1.2.3. M³ Optical Periods

[7] Here we refer to two distinct periods of M³ operations: OP1B and OP2C1. These two periods are discussed in more detail by *Boardman et al.* [2011], but can be summarized by the following: Data from OP1B were acquired from the 100 km orbit, with relatively low Sun angles, relatively low detector temperatures, and thus relatively low noise levels, but relatively low signal levels. Data from OP2C1 were

acquired from the 200 km orbit, at high Sun angles, high detector temperatures, high noise levels, but high signal levels. Data from OP1B are referred to as “cold,” and data from OP2C1 are referred to as “warm” or “hot,” due to the temperature of the M³ detector during these periods, as illustrated in Figure 1.

1.3. M³ Data Artifacts Resulting from Variable Operational Conditions

[8] Largely as a result of operating over such extreme conditions for which reliable laboratory calibration data are not available, significant artifacts were observed in the M³ level 1B (radiance) data. Many of the spectral artifacts were addressed in the level 2 (reflectance) calibration, but as with many corrections to spectral reflectance data, residual artifacts remain. We do not discuss every artifact and correction or the full details of the level 2 calibration sequence (these details are provided by other authors, including *Clark et al.* [2011], *Hicks et al.* [2011], and *Besse et al.* [2011a]), but we discuss a few with especially prominent implications for the necessity of a ground truth correction (discussed in more detail below).

[9] First, calibrated M³ reflectance spectra of mature lunar soils vary subtly (particularly in absorption band strength and shape) from the optical properties of lunar soils known from decades of laboratory study. After calibration to radiance, numerous systematic band-to-band artifacts were observed in M³ spectra. These were corrected using a technique termed “statistical polishing” by the M³ team. The full procedure is provided in the M³ software interface specification document (SIS) delivered with the M³ PDS archive [*Lundeen et al.*, 2011; *Malaret et al.*, 2011], but is summarized here. The full M³ data set was searched for spectra exhibiting the weakest absorption features under instrument “warm” and instrument “cold” conditions (conditions as discussed above). The resulting two sets of spectra were averaged and fit with cubic splines. These cubic splines were fit to follow low-frequency curvature of the spectra. The ratio between the average spectra and the cubic spline fits produces the multiplicative spectral polisher. This procedure had the desired effect of removing significant band-to-band artifacts in the M³ reflectance data. However, the spline fitting procedure had the effect of altering the very weak absorption features typical of mature lunar soils (the spline fits could not fit these features perfectly, so the “statistical polishing” step has the effect of minimizing very subtle absorption features). Thus, the M³ reflectance data differ slightly from the spectral properties of lunar soils as known from decades of laboratory study [e.g., *Adams and McCord*, 1971; *Hapke et al.*, 1975; *Noble et al.*, 2001; *Pieters*, 1999; *Pieters et al.*, 1993; *Pieters et al.*, 2000; *Taylor et al.*, 2001; *Taylor et al.*, 2010]. This variation can be observed in the example spectra illustrated in Figure 2, which includes uncorrected spectra from common locations between OP1B and OP2C1 (dotted lines) as well as the corrected versions (solid lines).

[10] Second, M³ observations of the same terrain under different operational conditions do not produce identical reflectance spectra. A fairly prominent artifact was observed in which spectral features consistent with the overall spectral shape of the raw level 0 signal (measured DN) appeared in the calibrated radiance (level 1B) signal. This artifact was

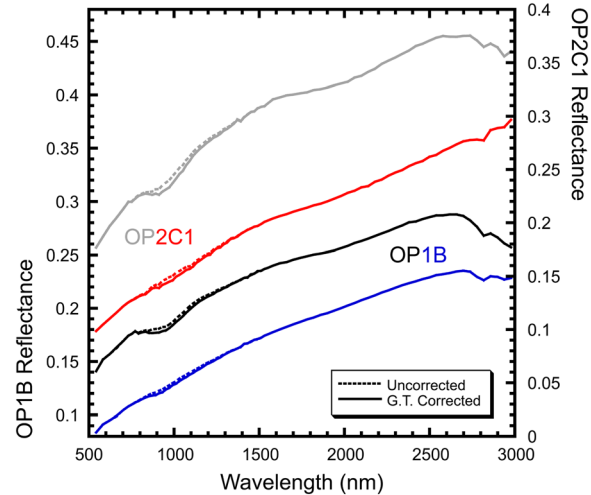


Figure 2. Example M³ spectra from common locations acquired during OP1B and OP2C1 (offset reflectance axes). Spectra are shown both before (dotted lines) and after (solid lines) application of the ground truth correction. The “before” spectra are M³ level 2 spectra as found in the PDS archive, whereas the “after” spectra have the ground truth correction applied to the as-delivered (to the PDS) spectra. Prior to application of the ground truth correction, mature soil spectra (lower plot in each set) are essentially featureless across the 1 μm region, particularly the OP2C1 data. After application of the ground truth correction, the 1 μm ferrous absorption is much closer to the known properties of mature lunar soils as measured in the laboratory. Spectra with stronger absorption features (upper plot in each set), are not changed as dramatically by the ground truth correction (the shape is not altered as dramatically), and only a minor change in absolute band strength is affected. Note that the ground truth correction does not change absolute albedo or continuum slope.

observed most prominently when comparing data acquired over the same location but under variable instrument thermal states; a spectral ratio of such observations should be flat (1.0 for every spectral channel, assuming no change in the surface between observations), but such comparisons between M³ data acquired under different instrument thermal states exhibited features consistent with the shape of the raw DN signal. Data acquired when the detector was “cold” (i.e., OP1B/2A and late in OP2C) exhibit these features more prominently. This artifact and the variability in M³ data collected under different conditions are likely driven largely by external thermal conditions; M³ is itself quite stable (observing the same terrain under similar instrument conditions *does* result in similar spectral properties) [*Green et al.*, 2011; *Rodriguez et al.*, 2009].

[11] The M³ team was not able to identify conclusively the root cause of this variability between data collected under different conditions, but was able to develop an empirical correction based on enforcing this “flat spectral ratio” condition (expected for ideal measurements) for data collected over the same region but under a range of observation conditions. There are several limitations to this approach, including the fact that it ignores effects of differential viewing geometries (phase angles) and that it corrects both “varieties” of M³ data

(i.e., “cold” and “warm” detector environments) to be the same, but does not assume either one is “correct.” Rather, the correction modifies both varieties to an intermediate point between the two behaviors. This fix (called the “smooth shape correction”) and the other elements of the level 2 calibration procedure are discussed more thoroughly in the M³ SIS [Lundeen *et al.*, 2011; Malaret *et al.*, 2011]. While this correction does improve the data set, it is not perfect, and residual artifacts are present in the data. Despite the “smooth shape correction,” calibrated M³ reflectance data collected under different conditions exhibit subtle differences in the ferrous 1 μm absorption band. This means that in addition to M³ spectra varying from known properties of lunar materials based on laboratory study (as discussed above), M³ data collected over the same region but under different operational conditions could indicate different surface properties if a correction for this variability is not applied.

1.4. Ground Truth Correction of Lunar Data Sets

[12] Extensive laboratory spectroscopic study of lunar soils has led to a detailed understanding of the optical properties of lunar soil [e.g., Taylor *et al.*, 2001; Taylor *et al.*, 2010]. This detailed understanding means that laboratory spectral data can be used as “ground truth” for calibration of remote data sets [e.g., Pieters, 1999]. While lunar soil samples are not ideal ground truth materials due to the need to extrapolate from small samples collected from precise locations to relatively large remote sensing “pixels”, lunar regolith is assumed to be sufficiently compositionally homogeneous on the scale of M³ data ($\sim 10^2$ m) to justify this extrapolation. Ground truth corrections can take a variety of forms, ranging from use as the primary calibration method for remote data sets or as minor adjustments to radiometrically calibrated (based on pre-flight instrument-specific laboratory calibration measurements) data sets. For example, Earth-based visible to near-infrared telescopic lunar observations relied on laboratory data for absolute calibration (measurements were taken relative to a standard site, and the absolute spectral shape was provided by the ground truth correction) [McCord *et al.*, 1981; Pieters, 1978, 1986]. Lunar orbital data sets have relied on ground truth data to enable fine-tuning of absolute radiometric calibration [e.g., Kieffer and Stone, 2005; McEwen *et al.*, 1998; Ohtake *et al.*, 2010; Pieters, 1999]. The typical reference standard used is the *Apollo 16* soil sample 62231, because of its high degree of maturity (roughly interpretable as “degree of weathering,” indicated by the parameter Is/FeO [e.g., Morris, 1976; 1978; Taylor *et al.*, 2001; Taylor *et al.*, 2010]) and the fact that it has been very well characterized [e.g., Fischer and Pieters, 1994; Pieters, 1999; Taylor *et al.*, 2001; Taylor *et al.*, 2010]. Ground truth corrections using laboratory measurements carry an implicit assumption that the sample measured in the laboratory is directly representative of the surface material observed in the remote measurements [e.g., Clark *et al.*, 2002]. The high degree of maturity of the 62231 soil sample makes this a more reasonable assumption, as typical lunar surfaces are covered with mature lunar soil. Additionally, global estimates of chemical composition and mineralogy indicate that the 62231 soil is broadly representative of “typical” lunar feldspathic highland soils [e.g., Jolliff *et al.*, 2000; Pieters, 1986].

1.5. The Feldspathic Highlands Terrane

[13] We discuss the feldspathic highlands terrane (FHT) in detail because we will use a subset of this terrane as a test case for a ground truth correction developed for the M³ reflectance data set. The FHT is one of three major lunar crustal terranes defined by Jolliff *et al.* [2000] based primarily on orbital estimates of bulk chemistry [e.g., Lawrence *et al.*, 1998; Lucey *et al.*, 1998]. Specifically, the FHT is characterized by both low FeO and Th abundance. Jolliff *et al.* [2000] characterized the FHT as being largely anorthositic, although it was further subdivided with a central subregion (FHT-An) that is especially anorthositic in composition based upon its high albedo and low FeO content (mean estimated FeO abundance of 4.2 wt% [Jolliff *et al.*, 2000]). Analyses of crater central peaks in the FHT region (outside of regions dominated by basaltic materials filling large impact basins) indicate that the terrane is largely anorthositic to substantial depth (~ 40 km) [Cahill *et al.*, 2009; Tompkins and Pieters, 1999]. This central anorthositic region of the FHT is roughly located in the northern lunar farside highlands, in a region where some of the thickest crust on the Moon is found [e.g., Ishihara *et al.*, 2009]. Evidence from returned lunar samples and lunar meteorites indicates that the feldspathic materials in the FHT have relatively ferroan compositions (high Fe/(Fe + Mg)), although lunar meteorites and global remote sensing data sets suggest that feldspathic highland materials may be more compositionally diverse than the ferroan anorthosites collected from the *Apollo 16* site [e.g., Jolliff *et al.*, 2000; Korotev *et al.*, 2003; Pieters *et al.*, 1983].

2. Development of the M³ Ground Truth Correction

[14] The reference standard spectrum and the ground truth correction developed by the M³ team are discussed in full in the M³ SIS document [Lundeen *et al.*, 2011; Malaret *et al.*, 2011]. We summarize that discussion here. The ground truth correction derived for M³ is based on laboratory spectroscopic measurements of *Apollo 16* soil sample 62231 [Pieters, 1999] and M³ observations of many mature feldspathic highland regions. Differences in viewing geometry, surface texture, and other observation conditions can have significant effects on many parameters related to VNIR spectra, but among the most important are effects on the continuum slope and absolute albedo. Additionally, laboratory measurements are known to vary systematically from remote measurements, particularly in absolute albedo [e.g., Blewett *et al.*, 1997; Hillier *et al.*, 1999; Ohtake *et al.*, 2010; Shkuratov *et al.*, 2000; Staid and Pieters, 2000]. Thus, the M³ ground truth correction was formulated to correct band strength, shape, and position while not affecting albedo and continuum slope. Derivation of a ground truth correction that does not affect overall albedo and continuum slope required the removal of a continuum slope from the M³ and laboratory data using the same methodology. The approach employed by the M³ team was to use a convex hull continuum slope composed of straight-line segments between local spectral maxima. After continuum removal, the laboratory reference standard spectrum was further modified using a convolution smoothing filter to address band-to-band artifacts. Additionally, because laboratory

measurements of truly anhydrous lunar soils are not available (even when measured under dry-air purged conditions, minor absorptions due to water are observed in lunar soil spectra [e.g., Isaacson, 2010]), a fit to the spectrum obtained using the Modified Gaussian Model (MGM) [Sunshine et al., 1990] was used in place of the continuum-removed measured data over the 1500–2500 nm range. From 2500 nm to 3000 nm, the reference standard was set to 1.0 so as not to impart any bias in the hydration absorption features found in this wavelength region [e.g., Clark et al., 2007]. The final reference standard spectrum is illustrated in Figure 3.

[15] The M³ ground truth correction was derived by averaging calibrated reflectance spectra from a number of small regions across the feldspathic highlands and regressing the resulting average against the reference standard spectrum. Separate correction factors were derived for data collected under the “cold” and “warm” distinct operational conditions of M³. The M³ ground truth correction described here and in the M³ SIS corrects only wavelengths below ~1500 nm. This limitation is driven primarily by residual calibration and/or thermal effects at wavelengths above ~1500 nm which cause the “cold” and “warm” M³ spectra from which the correction factors were derived not to converge at any wavelength beyond the critical 1 μm region. Thus, any correction to a single reference standard at wavelengths above ~1500 nm would involve unacceptable changes to the spectral shape, which is the basis for compositional assessments using the data set. This situation is illustrated by Figure 3, which shows the average M³ “cold” and

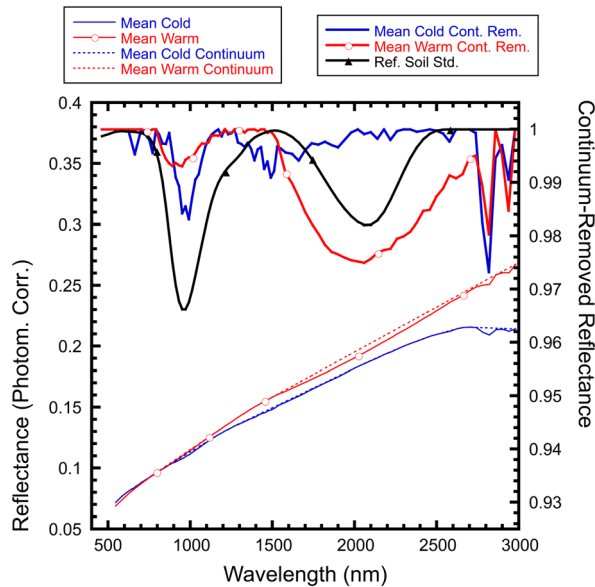


Figure 3. Average M³ spectra for mature highland soils used to derive the ground truth correction for warm and cold detector conditions. The average photometrically corrected reflectance spectra and continuum slopes are shown in thin solid and dotted lines, respectively, and the continuum removed spectra in heavy solid lines. The reference standard spectrum is shown only as continuum removed. The substantial divergence between the “cold” and “warm” spectra in the 2 μm region prevented the M³ team from deriving an acceptable ground truth correction that extended beyond 1500 nm.

“warm” spectra used to derive the correction and the continuum removal process. The M³ ground truth correction is derived only for wavelengths below 1500 nm because of the unacceptable divergence of the “cold” and “warm” spectra in the broad 2000 nm region, likely linked to residual thermal/calibration effects in the “warm” spectra (note the prominent apparent 2000 nm “absorption”). The ground-truth correction factors (G.T.) are illustrated in Figure 4.

[16] The M³ ground truth factors are applied as spectral multipliers; the method is given by equation (1):

$$R_{GT}(\lambda) = R_{L2}(\lambda) * GTF(\lambda) \quad (1)$$

where R_{GT} is ground truth-corrected reflectance, R_{L2} is the reflectance product available in the M³ level 2 archive (photometrically corrected reflectance), and GTF is the ground truth factor (different factors for “cold” and “warm” detector temperatures). The validity of a strict ground truth correction for the M³ data set is provided in part by comparison to other orbital lunar data sets such as the Kaguya Spectral Profiler, which exhibits 1 μm absorption band strengths and shapes for feldspathic lunar soils comparable to the 62231 laboratory soil spectrum in data collected near the *Apollo 16* landing site (e.g., Ohtake, M., et al., One Moon, many measurements 3: Spectral reflectance, *Icarus*, submitted; Matsunaga, personal communication).

[17] Example before- and after-correction spectra are shown in Figure 2. Average spectra from the study area (typical of feldspathic highlands materials) are shown in Figure 5. In both cases, the spectra were acquired from the same locations, but were acquired under the two different operational conditions of M³ described above (OP1B and OP2C1). The average spectra were collected from the study area clipped to a maximum latitude of 60°N, with null pixels and outliers removed. Outliers were defined as any spectrum with a reflectance value at any wavelength lying beyond two

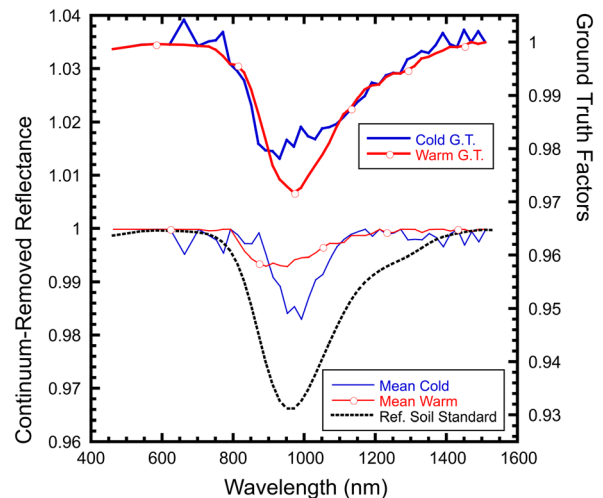


Figure 4. M³ ground truth correction spectral multipliers. The lower spectra (left axis) are the same as those (continuum-removed) spectra shown in Figure 1. The upper “spectra” (right axis) are the ground truth correction spectral multipliers derived for the two operational “conditions” of the M³ data set. They were derived by regressing the continuum-removed M³ average spectra (thin lines) against the reference standard spectrum (dotted line).

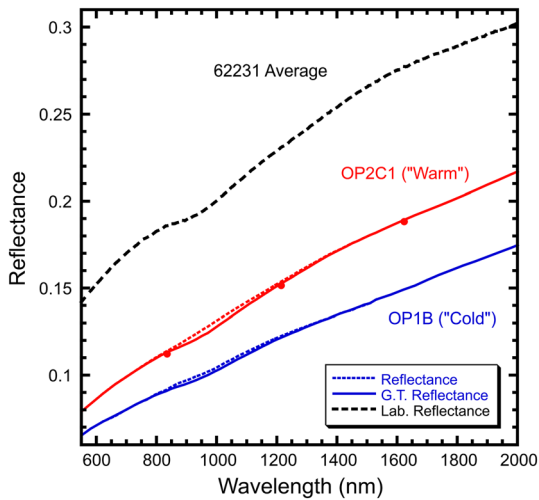


Figure 5. Mean M³ reflectance spectra of the study area. Spectra are shown for OP1B and OP2C1, with and without the ground truth (G.T.) correction applied. The M³ spectra are averages of the entire study area, below 60°N. For comparison, the 62231 average spectrum [Pieters, 1999] used as a typical ground truth reference standard is shown on the same axes. These spectra can be compared directly to those in Figure 3, which are from small regions within the study area.

standard deviations of the mean value at that wavelength (i.e., an outlier reflectance value at any single wavelength was sufficient to define an entire spectrum as an “outlier”). These average spectra illustrate how the ground truth correction brings these spectra into closer consistency (in strength, shape, and absorption band position) with laboratory spectra of lunar soils, an example of which is shown on the same axes in Figure 5 for comparison. These spectra also illustrate the variability in spectral properties between M³ data collected under different operational and observational conditions, as the region covered in these average spectra is identical but the spectral properties are not.

[18] The ground truth correction is not applied to the M³ data by the calibration pipeline in producing the level 2 data set delivered to the PDS [Lundeen *et al.*, 2011; Malaret *et al.*, 2011], but is provided with the archive as a set of wavelength-dependent multipliers to enable users to apply the correction themselves after evaluating its importance for their particular investigation. The correction factors can be found in the calibration (CALIB) directory of the M³ level 2 PDS archive (http://pds-imaging.jpl.nasa.gov/data/m3/CH1M3_0004/CALIB/) and can be identified by the “RFL_GRND_TRU” suffix in the file name. The specific ground truth correction factor file to use with a particular M³ file is indicated by the date ranges in the PDS label (.LBL) files.

[19] The ground truth correction will have significant effects only for relatively weak absorption features; strong features like those typically associated with optically immature surfaces should be largely unaffected at the several percent absorption strength level (as demonstrated by Figure 2). However, regional/global studies are sensitive largely to lunar soils (which dominate the surface and have very weak absorption features), so the use of the ground truth correction must be carefully considered for such studies.

3. Analytical Methods: Band Strength Evaluations

[20] To evaluate the efficacy of the M³ ground truth correction, we developed a parameter to quantify the strength of the 1 μm ferrous absorption in M³ data. The parameter is an integrated band depth similar to that used in previous publications using M³ data [e.g., Besse *et al.*, 2011b; Isaacson *et al.*, 2011b; Klima *et al.*, 2011; Pieters *et al.*, 2011; Staid *et al.*, 2011]. The 1 μm band depth parameter is similar to the parameter used in previous publications in that it is calculated by fitting a linear continuum over the 1 μm feature and then summing the band depths relative to the continuum at each wavelength within the limits defined by the parameter formulation. However, our version of the parameter varies from these previous integrated band depths in the wavelengths used as tie points for the linear continuum and limits for the band depth summation (a narrower wavelength range for both); our parameter uses 770–1170 nm as continuum tie points and sums the band depths over that same interval, whereas the previous parameter used 699 nm and 1579 nm as continuum tie points and summed the band depths over 790 nm to 1309 nm. A general formulation of this parameter is given by equation (2):

$$1 \mu\text{m IBD} = \sum_{\lambda_1}^{\lambda_2} 1 - \frac{R(\lambda)}{R_c(\lambda)} \quad (2)$$

where $\lambda_1 = 770$ nm and $\lambda_2 = 1170$ nm. This modification was done to focus the analysis more specifically on the weak 1000 nm (pyroxene-dominated) absorption observed in spectra of lunar soils; the formulation used in previous studies covered an intentionally broad wavelength range in order to capture the ferrous 1000 nm absorption across a broad range of materials. Our parameter was calculated for M³ data that were rebinned to lower spatial resolution (by a factor of 10 in each spatial dimension, for a final resolution of ~ 1.4 km/pixel) covering the study region. This rebinning was performed for each of the conditions we studied, OP1B (low Sun, low signal, cold detector) and OP2C1 (high Sun, high signal, warm detector). In general, an integrated band depth parameter is sensitive to a range of variations in the total character of the ferrous 1 μm feature and is not necessarily a direct proxy for the maximum depth of the absorption (e.g., relatively weak but very broad absorptions could have a higher value than strong narrow absorptions). Thus, we also calculated a single channel band depth parameter relative to a continuum. The tie points used for the continuum slope were the same as those used in the integrated band depth parameter, and the band depth relative to the continuum was calculated at 970 nm. The band depths were calculated for each spatial pixel in the study area for each of the conditions studied.

3.1. Study Area and Data Sets

[21] Our study area is a subset of the FHT-An region and is illustrated in Figure 6, with a detailed view provided in Figure 7. This region was chosen for its compositional (and thus spectral) homogeneity and for its relative lack of strong spectral features (due to its feldspathic composition and optical maturity). Furthermore, this specific region of the FHT-An was selected because M³ data from both of

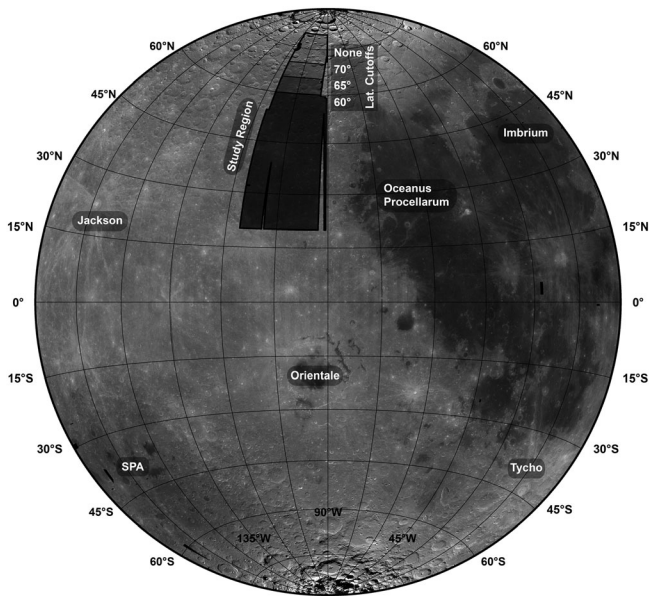


Figure 6. Illustration of the study area. The base map is Clementine UVVIS 750 nm albedo. The map is in a Lambert Azimuthal Equal Area projection after *Bussey and Spudis* [2004] centered on the western limb (longitude 90°W). Latitude and longitude coordinates are given by the thin lines and are in 15° increments. Selected major lunar morphological features are labeled for context. The study area is indicated, with the various maximum latitude cutoffs used in our analyses labeled and indicated by the different shading fills.

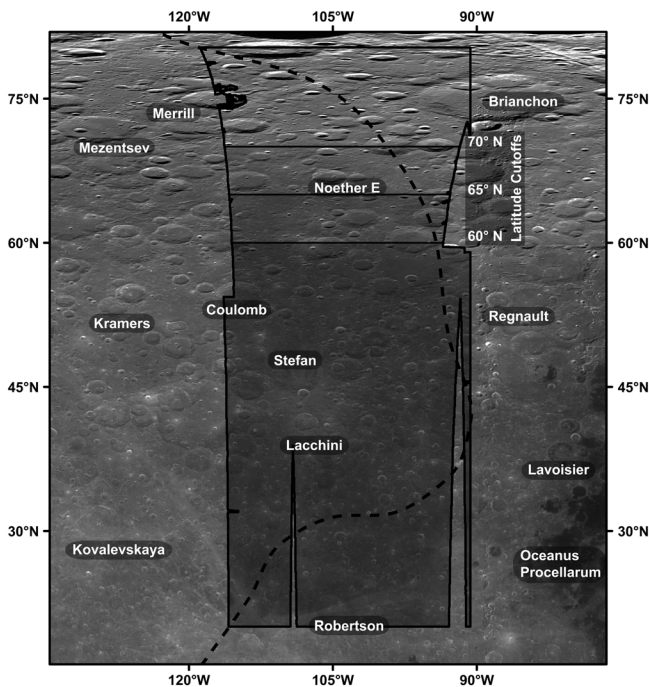


Figure 7. Detailed view of the study area. The study area and latitude cutoffs are illustrated as in Figure 6. The base map is the same image used in Figure 6. The map is in a simple cylindrical projection. The dashed line represents our interpretation of the approximate boundary of the FHT-An terrane as defined by *Jolliff et al.* [2000]. Selected lunar features are labeled for context.

the distinct operational conditions (cold and warm) cover the region. The M³ spectra collected from this region should be relatively featureless due to these properties, and thus the region is an excellent test case for the M³ ground truth correction. The parameters (equation (2) and the single-channel band depth) were calculated with and without the ground truth correction applied for each of the two operational conditions, for a total of four scenarios (OP1B with and without the ground truth correction, and OP2C1 with and without the ground truth correction). We clipped the calculated parameter maps to regions common to both periods as well as the approximate boundaries of the FHT-An of *Jolliff et al.* [2000] such that the summary results for the band strength analyses are from identical geographic regions within the FHT-An terrane. The final clipped region is provided in Figure 7.

[22] As in many orbital missions, signal levels in M³ data tend to decrease (and noise levels to increase) as latitude increases. Thus, we calculated our results for a series of subset regions, including the full study area and then the study area clipped to a maximum latitude of (i.e., the study area was restricted to regions with latitude less than) 70°N, 65°N, and 60°N, for a total of four analysis regions. These subset regions are illustrated in Figures 6 and 7. Because our study area is at relatively high latitudes, we also conducted spot test comparisons at lower latitudes of band depth parameters calculated from corrected (after application of the ground truth correction) and uncorrected data. However, these more equatorial regions are complicated by a higher abundance of immature materials and increased heterogeneity (e.g., the northern Orientale region). The increased complexity of these more equatorial regions causes the “signal” of the ground truth correction to be hidden to some degree by the “noise” imparted by these additional complicating factors.

[23] Because remote data such as those collected by M³ suffer from noise and artifacts, outliers are typically observed in regional analyses such as the one conducted here. We excluded extreme outliers (which are likely caused by residual calibration artifacts) using the definition provided previously (any reflectance value falling beyond two standard deviations from the mean). After the outliers were removed, basic statistics were calculated on the results (mean, minimum, maximum, and standard deviation). For context, we calculated statistics (for the same regions) on absolute FeO content of the near-surface materials based on data collected by the Lunar Prospector Gamma Ray Spectrometer instrument [*Lawrence et al.*, 2002]. The FeO abundance data are presented to assist in evaluating band strength results, as FeO abundance is one of the primary drivers of band strength variability in lunar reflectance data across the 1 μm region (in addition to variable optical maturity) [e.g., *Hapke*, 2001; *Le Mouélic et al.*, 2002; *Lucey et al.*, 2000a; *Lucey et al.*, 2000b; *Pieters et al.*, 2000; *Taylor et al.*, 2001; *Taylor et al.*, 2010].

[24] We evaluated the mean phase angles in the study area for the two different periods (OP1B and OP2C1) and found them to vary by ~20°, with OP1B having mean phase angles of ~60° in the study area and OP2C1 having mean phase angles of ~40°. The difference and exact value of the mean phase angle vary slightly with the cutoff latitude, but the difference is only a few degrees of phase angle, and at these

phase angles, approximate values are sufficient. The photometric correction derived by the M³ team and applied in creating the delivered level 2 data set is intended to account for variable phase angles [Besse *et al.*, 2013; Hicks *et al.*, 2011]. However, the phase angle difference is an important consideration for a few reasons. First, artifacts in the analysis could result from phase angle effects not accounted for by the photometric correction. Second, variable phase angles were not considered in deriving the shape correction. Additionally, differences in band strength as a function of phase angle are possible, although the effect of phase angle on absorption band strength is expected to be most significant at very high phase angles, and the difference in phase angles we observed for our study area is not expected to have a major impact on band strength at the phase angles observed in our area (Clark *et al.*, in preparation).

4. Results

[25] The principal results of the integrated band depth analyses are presented as basic statistics (mean, minimum, maximum, and standard deviation) of the calculated parameter for each of the four cases and four latitude subsets. These results as well as the same statistics for the FeO abundance (wt%) from Lunar Prospector are presented in Table 1. The results for the single-channel band depth parameter (band depth at 970 nm) are presented in Table 2. Note that some conditions return negative mean band strength values. This result is due to the parameter formulation and the average spectral shape in these regions. If spectra have substantial convexity across the 1 μ m region, negative band strengths or integrated band strengths can be obtained. If sufficient numbers of these spectra are included in the

Table 1. Results of Integrated 1 μ m Band Depth and Lunar Prospector FeO Analyses

Subset Region	Operational Condition ^a	Mean	Minimum	Maximum	Standard Deviation
Full	OP1B	-0.058	-2.442	2.207	0.361
	OP1B GT ^b	0.141	-2.101	2.269	0.348
	OP2C1	0.107	-2.013	2.237	0.274
	OP2C1 GT ^b	0.317	-1.902	2.555	0.272
	LP Fe ^c	5.861	4	7	0.794
Max. 70°N	OP1B	-0.005	-0.967	0.876	0.214
	OP1B GT ^b	0.191	-0.732	1.031	0.208
	OP2C1	0.020	-0.318	0.402	0.132
	OP2C1 GT ^b	0.231	-0.102	0.609	0.130
	LP Fe	5.767	4	7	0.768
Max. 65°N	OP1B	0.014	-0.787	0.740	0.181
	OP1B GT ^b	0.209	-0.546	0.889	0.175
	OP2C1	0.002	-0.282	0.326	0.114
	OP2C1 GT ^b	0.214	-0.067	0.534	0.113
	LP Fe	5.690	4	7	0.754
Max. 60°N	OP1B	0.025	-0.687	0.673	0.160
	OP1B GT ^b	0.220	-0.442	0.819	0.154
	OP2C1	-0.012	-0.262	0.273	0.102
	OP2C1 GT ^b	0.200	-0.047	0.481	0.100
	LP Fe	5.563	4	7	0.699

^aRefers to cold (low Sun, low signal, cold detector—OP1B) or warm (high Sun, high signal, warm detector—OP2C1) conditions.

^bBand depth parameter calculated on spectra after application of ground truth correction.

^cLP Fe refers to wt% FeO.

Table 2. Results of Single-Channel Band Depth at 970 nm

Subset region	Operational Condition ^a	Mean	Minimum	Maximum	Standard Deviation
Full	OP1B	0.002	-0.445	0.440	0.041
	OP1B GT ^b	0.017	-0.322	0.352	0.036
	OP2C1	0.010	-0.701	0.711	0.031
	OP2C1 GT	0.032	-0.519	0.581	0.029
Max. 70°N	OP1B	0.007	-0.070	0.078	0.016
	OP1B GT ^b	0.021	-0.054	0.091	0.016
	OP2C1	0.003	-0.030	0.039	0.013
	OP2C1 GT	0.025	-0.007	0.060	0.012
Max. 65°N	OP1B	0.007	-0.053	0.063	0.014
	OP1B GT ^b	0.022	-0.037	0.077	0.014
	OP2C1	0.001	-0.026	0.032	0.011
	OP2C1 GT	0.023	-0.003	0.054	0.011
Max. 60°N	OP1B	0.008	-0.041	0.053	0.013
	OP1B GT ^b	0.022	-0.026	0.067	0.013
	OP2C1	0.000	-0.024	0.028	0.010
	OP2C1 GT	0.022	-0.002	0.049	0.010

^aRefers to cold (low Sun, low signal, cold detector—OP1B) or warm (high Sun, high signal, warm detector—OP2C1) conditions.

^bBand depth parameter calculated on spectra after application of ground truth correction.

statistics, the mean value can have a negative value (note that these are largely observed for the higher latitude cutoffs). While the parameters were formulated to minimize these effects, the fundamental shape of the spectra in the M³ reflectance data set dictated that some negative values would be obtained. For comparison, the reference standard spectrum used to derive the M³ ground truth corrections has a value of 0.286 in the integrated band depth parameter, and a value of 0.0276 in the single-channel band depth at 970 nm. Note in particular that the standard deviation in band strength values is much lower for the lower latitude

cutoffs, most likely due to removal of more noisy spectra resulting from low signal levels and low signal-to-noise levels at the higher latitudes.

[26] Our results show that average band strengths in the region are relatively low, consistent with the region's highly feldspathic composition. The relatively weak bands are apparent in the spectra shown in Figure 5. The band strengths and efficacy of the ground truth correction are illustrated statistically in Figures 8 and 9. The mean band depth values for the study area are compared graphically in Figure 8. The distribution of values in the study area for the two parameters (using the 60°N latitude cutoff) is illustrated by the histograms in Figure 9. The results indicate that in the study area, the

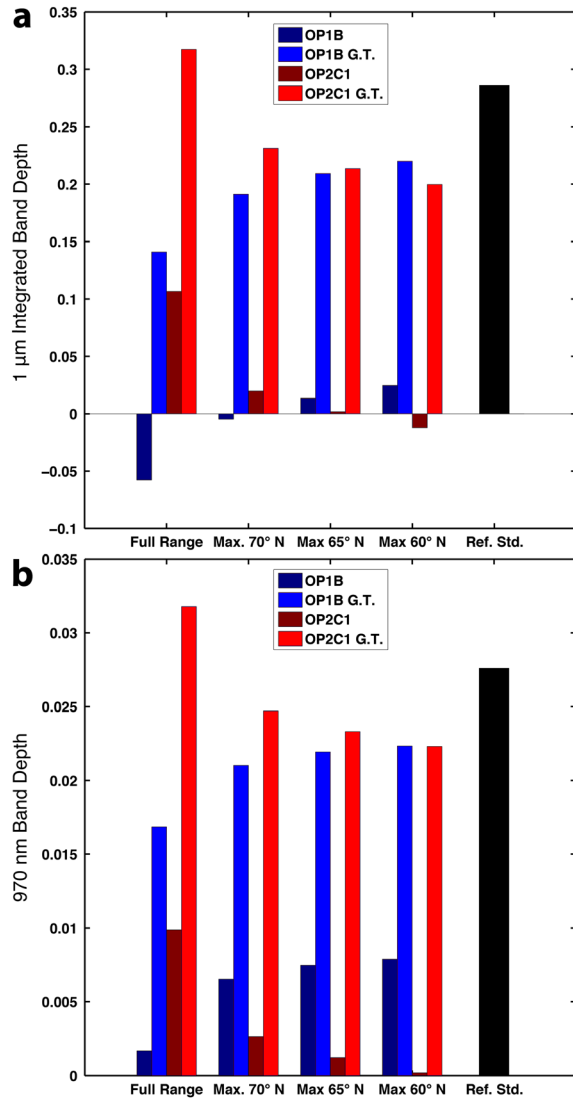


Figure 8. Comparison of average band depths for the integrated (a) 1 μm band depth parameter and (b) 970 nm band depth parameter. The four cases (OP1B and OP2C1, with and without ground truth (G.T.) correction) are compared as averages across the study region, with different maximum latitude cutoffs. At lower maximum latitude cutoffs where the extreme topography and lighting conditions at high latitudes are more minor factors, the ground truth correction brings the two data sets into very good agreement and brings them into closer agreement with the laboratory reference spectrum.

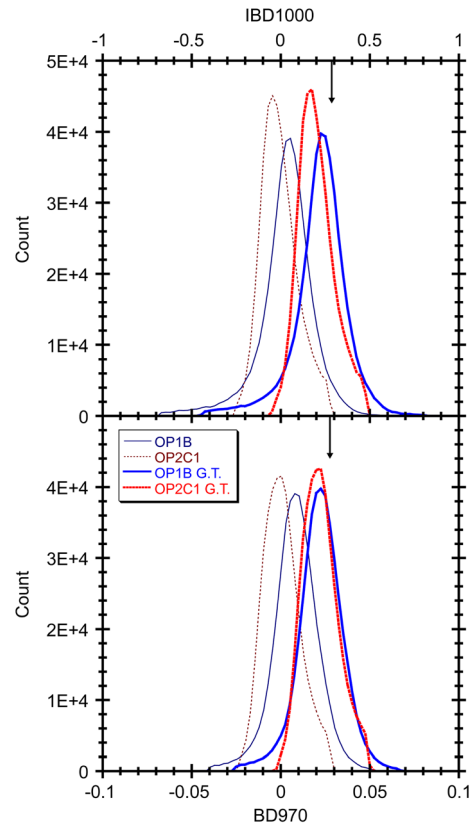


Figure 9. Distribution of band strength parameter values across the study region, using the 60°N maximum latitude cutoff. Distributions are shown both before (thin lines, lower BD values) and after (thick lines, higher BD values) application of the ground truth correction. This representation captures the variability of the band strength parameters across the study region, whereas Figure 8 captures only the mean values. The top panel illustrates the range in the IBD1000 (integrated band depth) parameter, and the bottom panel illustrates the range in the BD970 (single-channel band depth at 970 nm) parameter. The shapes of the histograms are broadly similar, although the IBD1000 parameter illustrates a broader spread (note the different x axis scales). This behavior is not surprising, as the IBD1000 parameter is sensitive to a broader range of spectral variability. The distributions are much closer after application of the ground truth correction, particularly for the BD970 parameter. The reference standard values are indicated by the arrows.

ground truth correction is successful at bringing the M³ data collected under different operational conditions into closer agreement with each other and with the reference standard. Our spot checks at more equatorial latitudes yield results consistent with the results from the study region, but as described above, the increased complexity of the more southern latitudes masks the signal of the ground truth correction to some degree.

5. Discussion

5.1. Variations Between Data Collected Under Different Conditions

[27] The results of the band depth analysis in the study region quantify observations that are apparent from qualitative evaluation of M³ spectra, as illustrated in Figures 2 and 5. Despite the best efforts of the M³ team in calibrating the acquired data, M³ data exhibit residual calibration effects that can largely be attributed to the widely varying and off-nominal operational conditions experienced by the Chandrayaan-1 spacecraft and M³. These challenges led to a variety of issues, but the variations in the strength, shape, and position of the 1 μm ferrous absorption feature are the principal focus of the present work. In considering the results of this study, it is important to recall that the regions studied under the two conditions (OP1B and OP2C1) were spatially identical and were observed less than 6 months apart, meaning they can be considered compositionally identical. This means that differences in composition (e.g., FeO and/or TiO₂ abundances) or in optical maturity cannot reasonably be invoked as explanations for differing spectral properties. The only substantial difference between the two conditions across the study area, other than the different thermal condition of M³, is a difference in viewing geometry. While the effects of viewing geometry on absolute band strengths are not well studied and some effects are expected [e.g., Clark, 2009], substantial variability in band strengths is expected only at extreme viewing geometries (e.g., very high incidence angles). The variations in the observed spectral properties therefore must be considered largely instrumental effects.

5.2. Strengths and Weaknesses of the M³ Ground Truth Correction

5.2.1. Improved Consistency Between Different Operational Conditions

[28] The most significant result to note concerns the difference between optical periods (disregarding the use or non-use of ground truth). Across all subsets of the study region, OP1B and OP2C1 exhibit significantly different 1 μm absorption strengths before the ground truth correction is applied. The absorption strength of the region is consistent with or less than the *Apollo 16* reference standard spectrum, depending on the observational condition and use of the ground truth correction. In other words, the maximum observed band strength of the conditions evaluated was on the order of the band strength of the reference standard spectrum. Other conditions produce a significantly weaker feature. We merely point out these important differences in the M³ data set, without advocating that one is strictly more “correct” than the others.

[29] The variability in band strength is illustrated both by the mean values displayed in Figure 8 and by the distributions of band strength values shown in Figure 9. The results are consistent across all of the geographic (latitude) cutoffs used. The absolute values change and the values vary slightly less as the higher latitudes are removed from the analysis (as stronger features near the poles, likely linked to spurious features and/or shadowing effects, are excluded), but the substantial differences between optical periods do not. The difference between OP1B and OP2C1 does vary between different latitude cutoffs, likely an effect of the different viewing geometries between the two optical periods and of low signal levels at high latitudes. There are slight differences in the iron abundance in the various subset regions, as shown by the Lunar Prospector FeO abundance values in Table 1, but these differences are minor and would not cause the range in values between the various subset regions. Because of the decreased signal levels at higher latitudes, we have more trust in the data restricted to lower latitudes (max. 60°N and 65°N). In these subset regions, data from OP1B exhibit stronger 1 μm absorption features than data from OP2C1.

[30] The results also indicate that the ground truth correction brings the observed band strengths into closer agreement (between the two optical periods) than without the ground truth correction applied. The ground truth correction does not bring the results into perfect agreement between OP1B and OP2C1, which is not a surprise. The ground truth correction was derived from a range of feldspathic highland materials over a large area, but used the *Apollo 16* soil as a reference standard and assumed that that reference standard was an accurate representation of the spectral properties of all mature feldspathic lunar soils. This is a reasonable but not perfect assumption, and deviations should be expected. Differences between the optical periods after application of the ground truth correction should also be expected due to residual uncompensated artifacts that the ground truth correction was never intended to address. The results are highly consistent between the integrated band depth and single-channel band depth parameters.

[31] The differences between uncorrected and corrected mean band strength values are highly consistent between the two parameters (Figure 8), as are the changes in the band strength distributions (Figure 9). The distribution of band strength values in both uncorrected and corrected data is much tighter in the BD970 parameter (note the different x axis scales in Figure 9). This behavior is not a surprise, as the IBD1000 parameter is sensitive to a much broader range of spectral variability.

5.2.2. Improved Consistency with Reference Standard

[32] The ground truth correction brings both OP1B and OP2C1 data into closer agreement with the *Apollo 16* reference standard spectrum. This closer agreement is well illustrated both by the mean values shown in Figure 8 as compared to the reference standard and the improved consistency between the band strength distributions and the reference standard values (indicated by arrows) in Figure 9. To achieve this result, the absolute band strength does increase significantly after applying the ground truth correction (see further discussion below). As other researchers have noted, significant differences in brightness and band strength can be expected for comparisons between laboratory and remote

measurements [e.g., Hillier *et al.*, 1999; Ohtake *et al.*, 2010; Shkuratov *et al.*, 2000; Staid and Pieters, 2000], so it is possible that the M³ ground truth correction produces an “overcorrection” in correcting the observed highland soils to the band strength of the laboratory reference standard. The correction would be an “overcorrection” primarily if it is invalid to assume that lunar soil measured in the laboratory is an appropriate analogue for lunar soils measured in situ, as discussed below.

[33] The improved consistency with the reference standard is perhaps not surprising given that the ground truth correction was derived primarily by forcing feldspathic regions of the Moon to match the reference standard spectrum. However, it is important to note that our study region is not the same as that used to define the ground truth correction. The close match between the study region and the reference standard is a result of the feldspathic composition of our study area being broadly similar to that of the regions used to define the ground truth correction. The fact that the ground truth correction causes the observed band strengths for both OP1B and OP2C1 to closely match that of the *Apollo 16* reference standard is also a confirmation that the ground truth correction is effective at minimizing the differences between OP1B and OP2C1 observations.

5.2.3. Implications for Compositional Analysis

[34] The differences observed between M³ data collected over the same region under different observational and operational conditions have significant implications for any analysis of M³ data that relies on regional evaluation/mapping of the strength of the 1 μm ferrous absorption (for example, production of mineral maps or maps of derived chemical composition such as FeO abundance). Specifically, use of M³ data collected under different observational conditions could produce different estimates for the derived compositional products. The magnitude of this problem is illustrated by the mixing analysis presented in the supplementary materials. The strength of the 1 μm absorption is tightly coupled to mineralogy, and the magnitude of the “cold” and “warm” ground truth corrections can be thought of as the “difference” in the data set between the two conditions. The mixing analyses presented in the supplementary material indicate that compositional estimates could be in error by several percent and vary as a function of composition (i.e., the error could have different magnitudes for different compositions). This conclusion implies that estimations of chemical abundances based on the 1 μm absorption strength (e.g., FeO abundance) would have comparable offsets/errors.

[35] Another way to consider the implications of the effects discussed here on compositional analyses is to consider the magnitude of the difference between the OP1B and OP2C1 data in light of the compositional data provided in Table 1 (Lunar Prospector FeO abundance). These values indicate that the composition (i.e., mineral or chemical abundance) is *constant* in the study area, but the differences between the optical periods would predict a difference of up to several percent in mineral abundance and in chemical abundance. The ground truth correction reduces the difference between the optical periods substantially, reducing the range in derived composition that would be produced from analysis of the different varieties of M³ data. It achieves this

result by enforcing an increase in absolute band strength, as discussed above. In our opinion, this change is justifiable based on known properties of lunar soil from laboratory study. However, this conclusion carries an implicit assumption that lunar soil in the laboratory is a good analogue for in situ lunar soil. As this may not be a perfect assumption due to the inability of laboratory measurements to perfectly recreate in situ conditions [e.g., Blewett *et al.*, 1997; Carrier *et al.*, 1991; Hapke and van Horn, 1963; Hillier *et al.*, 1999], individual users must consider the use of the ground truth correction for their particular application.

[36] We also point out that compositional analyses done with data from a single operational condition (i.e., “cold only” or “warm only”) will not suffer from such variability; M³ was proved to be quite stable such that when operated under relatively constant conditions, the character of the acquired data did not exhibit substantial variability for similar surface materials. That is not to say that the M³ data set is entirely free from artifacts under such conditions, just that the prominent variability between operational conditions discussed here is not observed. However, the other motivation for the use of the ground truth correction (lack of similarity between observations of mature feldspathic regions and laboratory measurements of mature feldspathic lunar soils, implying systematic errors in band strength without the use of the ground truth correction) still holds, so users of M³ data should still consider use of the ground truth correction even if not making comparisons between data collected under the different operational conditions.

5.2.4. Limitations

[37] One of the most significant limitations of the M³ ground truth correction is its inability to correct wavelengths above 1500 nm. The reasons for this limitation are discussed above, but primarily result from two factors. First, the character of the M³ data under different observational conditions (“cold” versus “warm/hot”) is very different for wavelengths above 1500 nm and the two do not converge sufficiently to allow a reasonable correction; a correction would impose changes of unacceptable magnitude in this region. Second, a reliable reference standard at long wavelengths is very difficult to obtain without making substantial assumptions about the reflectance properties of in situ lunar soils, particularly with regard to the presence of hydrated species. The M³ ground truth correction does impart a significant change to the character (strength and shape) of the 1 μm ferrous absorption feature, which could be considered a limitation. However, because the changes cause the M³ data to be more consistent with the known properties of lunar soil from laboratory study, we view this change as a strength. However, when combined with the first limitation (limited wavelength range), the issues with changes to band shape and strength become substantial; comparisons of relative band strength and/or shape between the 1 μm region and longer-wavelength regions (e.g., the 2 μm absorption features of pyroxenes and spinels) will be biased by the use of the M³ ground truth correction. However, we view the ground truth correction as an important element for studies that rely primarily on the 1 μm absorption feature and wavelengths below \sim 1500 nm. Furthermore, we caution users making comparisons between the 1 μm and longer wavelength regions with M³ data about the prominent variability observed between the different operational conditions experienced by M³,

and recommend confining such analyses to a single range (either warm or cold data) if possible.

6. Conclusions

[38] Substantial differences are observed between M³ data collected from the same geographic region under different operational conditions of the Chandrayaan-1 spacecraft and the M³ instrument. The application of the ground truth correction delivered with (but not applied to) the M³ level 2 data set mitigates the variability in spectral properties between data collected under these different operational conditions. The ground truth correction also brings the M³ level 2 reflectance spectra into closer agreement with the known properties of lunar soils based on decades of careful laboratory analysis. The 1 μm ferrous absorption feature strengths in the studied region are quite low overall (on the order of 1–2%), similar to or weaker than absorption strengths in laboratory spectral measurements of *Apollo 16* soil samples. This is consistent with previous results and the highly feldspathic nature of the region. Users of M³ data are strongly advised to consider these issues carefully in selecting the data and calibrations to be used in their analyses, particularly for studies involving regional mapping of 1 μm ferrous absorption strength, or else risk significant errors in derived parameters such as mineral or chemical abundances. Synthetic mixture calculations demonstrate that errors of at least several percent can be expected if these issues are not addressed. Erroneous scientific conclusions could result, as major conclusions about lunar geology are frequently based on subtle differences in chemistry or mineralogy at the percent level. However, the ground truth correction is not able to correct wavelengths beyond $\sim 1500\text{ nm}$, so use of this correction for comparisons between the 1 and 2 μm regions should be done with caution. This limitation of the ground truth correction is an important area for future work.

[39] **Acknowledgments.** The efforts of the entire M³ engineering, operations, science, and data archiving teams are gratefully acknowledged. M³ science validation is supported through NASA contract NNM05AB26C. M³ is supported as a NASA Discovery Program mission of opportunity. The M³ team is grateful to ISRO for the opportunity to fly as a guest instrument on Chandrayaan-1. The authors thank Joshua Cahill, Bruce Hapke, and an anonymous reviewer for their thorough reviews and comments on this manuscript. The manuscript is much improved thanks to their constructive criticism. This is HIGP Publication 1919 and SOEST Publication 8539.

References

Adams, J. B. (1974), Visible and near-infrared diffuse reflectance spectra of pyroxenes as applied to remote sensing of solid objects in the solar system, *J. Geophys. Res.*, *79*, 4829–4836, doi:10.1029/JB079i032p04829.

Adams, J. B., and T. B. McCord (1971), Alteration of lunar optical properties: Age and composition effects, *Science*, *171*(3971), 567–571, doi:10.1126/science.171.3971.567.

Besse, S., J. Boardman, J. Nettles, M. Staid, J. M. Sunshine, J. Y. Li, Y. Yokota, B. Buratti, M. Hicks, and C. Pieters (2011a), Deriving a photometric model for the Moon Mineralogy Mapper data (M³), *Lunar Planet. Sci.*, *42*, 1773.

Besse, S., J. M. Sunshine, M. I. Staid, N. E. Petro, J. W. Boardman, R. O. Green, J. W. Head, P. J. Isaacson, J. F. Mustard, and C. M. Pieters (2011b), Compositional variability of the Marius Hills volcanic complex from the Moon Mineralogy Mapper (M³), *J. Geophys. Res.*, *116*(E00G13), doi:10.1029/2010JE003725.

Besse, S., J. Sunshine, M. Staid, J. Boardman, C. Pieters, P. Guasqui, E. Malaret, S. McLaughlin, Y. Yokota, and J. Y. Li (2013), A visible and near-infrared photometric correction for Moon Mineralogy Mapper (M³), *Icarus*, *222*(1), 229–242, doi:10.1016/j.icarus.2012.10.036.

Blewett, D. T., P. G. Lucey, B. R. Hawke, G. G. Ling, and M. S. Robinson (1997), A comparison of Mercurian reflectance and spectral quantities with those of the Moon, *Icarus*, *129*(1), 217–231, doi:10.1006/icar.1997.5785.

Boardman, J. W., C. M. Pieters, R. O. Green, S. R. Lundeen, P. Varanasi, J. Nettles, N. Petro, P. Isaacson, L. A. Taylor, and S. Besse (2011), Measuring moonlight: An overview of the spatial properties, lunar coverage, selenolocation and related level 1B products of the Moon Mineralogy Mapper, *J. Geophys. Res.*, *116*(E00G14), doi:10.1029/2010JE003730.

Burns, R. G. (1993), *Mineralogical Applications of Crystal Field Theory*, 2nd ed., 551 pp., Cambridge University Press, New York.

Bussey, B., and P. D. Spudis (2004), *The Clementine Atlas of the Moon*, 376 pp., Cambridge University Press, Cambridge, UK.

Cahill, J. T. S., P. G. Lucey, and M. A. Wicczorek (2009), Compositional variations of the lunar crust: Results from radiative transfer modeling of central peak spectra, *J. Geophys. Res.*, *114*, doi:10.1029/2008je003282.

Carrier III, W. D., G. R. Olhoeft, and W. W. Mendell (1991), Physical properties of the lunar surface, in *Lunar Sourcebook—A User's Guide to the Moon*, edited by G. H. Heiken, D. T. Vaniman and B. M. French, pp. 475–594, Cambridge University Press, Cambridge, England.

Clark, B. E. (1995), Spectral mixing models of S-type asteroids, *J. Geophys. Res.*, *100*, 14443–14456, doi:10.1029/95JE00720.

Clark, R. N. (2009), Detection of adsorbed water and hydroxyl on the Moon, *Science*, *326*(5952), 562–564, doi:10.1126/science.1178105.

Clark, R. N., C. M. Pieters, R. O. Green, J. W. Boardman, and N. E. Petro (2011), Thermal removal from near-infrared imaging spectroscopy data of the Moon, *J. Geophys. Res.*, *116*(E00G16), doi:10.1029/2011JE004044.

Clark, R. N., G. A. Swayze, R. Wise, E. Livo, T. Hoefen, R. Kokaly, and S. J. Sutley (2007), USGS digital spectral library splib06a, *USGS Digital Data Series 231*.

Clark, R. N., G. A. Swayze, K. E. Livo, R. F. Kokaly, T. V. V. King, J. B. Dalton, J. S. Vance, B. W. Rockwell, T. Hoefen, and R. R. McDougal (2002), Surface reflectance calibration of terrestrial imaging spectroscopy data: A tutorial using AVIRIS, paper presented at 10th Airborne Earth Science Workshop, JPL Publication 02-1.

Cloutis, E. A., and M. J. Gaffey (1991), Pyroxene spectroscopy revisited: Spectral-compositional correlations and relationship to geothermometry, *J. Geophys. Res.*, *96*(E5), 22809–22826, doi:10.1029/91JE02512.

Fischer, E. M., and C. M. Pieters (1994), Remote determination of exposure degree and iron concentration of lunar soils using VIS-NIR spectroscopic methods, *Icarus*, *111*(2), 475–488, doi:10.1006/icar.1994.1158.

Goswami, J. N., and M. Annadurai (2009), Chandrayaan-1: India's first planetary science mission to the moon, *Curr. Sci. India*, *96*(4), 486–491.

Green, R. O., et al. (2011), The Moon Mineralogy Mapper (M³) imaging spectrometer for lunar science: Instrument description, calibration, on-orbit measurements, science data calibration and on-orbit validation, *J. Geophys. Res.*, *116*(E00G19), doi:10.1029/2011JE003797.

Hapke, B. (2001), Space weathering from Mercury to the asteroid belt, *J. Geophys. Res.*, *106*, 10039–10074, doi:10.1029/2000JE001338.

Hapke, B., and H. van Horn (1963), Photometric studies of complex surfaces, with applications to the Moon, *J. Geophys. Res.*, *68*, 4545–4570.

Hapke, B., W. Cassidy, and E. Wells (1975), Effects of vapor-phase deposition processes on the optical, chemical, and magnetic properties of the lunar regolith, *Moon*, *13*, 339–353.

Hazen, R. M., P. M. Bell, and H. K. Mao (1978), Effects of compositional variation on absorption spectra of lunar pyroxenes, *Proc. Lunar Planet. Sci.*, *9*, 2919–2934.

Hicks, M. D., B. J. Buratti, J. Nettles, M. I. Staid, C. M. Pieters, J. M. Sunshine, S. Besse, and J. W. Boardman (2011), A photometric function for analysis of lunar images in the visual and infrared based on Moon Mineralogy Mapper observations, *J. Geophys. Res.*, *116*(E00G15), doi:10.1029/2010JE003733.

Hillier, J. K., B. J. Buratti, and K. Hill (1999), Multispectral photometry of the Moon and absolute calibration of the Clementine UV/Vis Camera, *Icarus*, *141*(2), 205–225, doi:10.1006/icar.1999.6184.

Hiroi, T., and C. M. Pieters (1994), Estimation of grain sizes and mixing ratios of fine powder mixtures of common geologic minerals, *J. Geophys. Res.*, *99*, 10867–10880, doi:10.1029/94JE00841.

Isaacson, P. J. (2010), *Lunar Sample Ground Truth: A Cornerstone of Remote Mineralogical and Compositional Analysis of Planetary Surfaces*, 338 pp., Brown University, Providence, RI.

Isaacson, P. J., A. Basu Sarbadhikari, C. M. Pieters, R. L. Klima, T. Hiroi, Y. Liu, and L. A. Taylor (2011a), The lunar rock and mineral characterization consortium: Deconstruction and integrated mineralogical, petrologic, and spectroscopic analyses of mare basalts, *Meteorit. Planet. Sci.*, *46*, 228–251, doi:10.1111/j.1945-5100.2010.01148.x.

Isaacson, P. J., et al. (2011b), Remote compositional analysis of lunar olivine-rich lithologies with Moon Mineralogy Mapper (M³) spectra, *J. Geophys. Res.*, *116*(E00G11), doi:10.1029/2010JE003731.

Ishihara, Y., S. Goossens, K. Matsumoto, H. Noda, H. Araki, N. Namiki, H. Hanada, T. Iwata, S. Tazawa, and S. Sasaki (2009), Crustal thickness

- of the Moon: Implications for farside basin structures, *Geophys. Res. Lett.*, *36*, 19202, doi:10.1029/2009GL039708.
- Jolliff, B. L., J. J. Gillis, L. A. Haskin, R. L. Korotev, and M. A. Wieczorek (2000), Major lunar crustal terranes: Surface expressions and crust-mantle origins, *J. Geophys. Res.*, *105*(E2), 4197–4216, doi:10.1029/1999JE001103.
- Kieffer, H. H., and T. C. Stone (2005), The spectral irradiance of the Moon, *Astronomical Journal*, *129*, 2887–2901, doi:10.1086/430185.
- Klima, R. L., C. M. Pieters, and M. D. Dyar (2007), Spectroscopy of synthetic Mg-Fe pyroxenes I: Spin-allowed and spin-forbidden crystal field bands in the visible and near-infrared, *Meteorit. Planet. Sci.*, *42*, 235–253, doi:10.1111/j.1945-5100.2007.tb00230.x.
- Klima, R. L., et al. (2011), New insights into lunar petrology: Distribution and composition of prominent low-Ca pyroxene exposures as observed by the Moon Mineralogy Mapper (M³), *J. Geophys. Res.*, *116*, E00G06, doi:10.1029/2010JE003719.
- Korotev, R. L., B. L. Jolliff, R. A. Zeigler, J. J. Gillis, and L. A. Haskin (2003), Feldspathic lunar meteorites and their implications for compositional remote sensing of the lunar surface and the composition of the lunar crust, *Geochim. Cosmochim. Acta*, *67*(24), 4895–4923, doi:10.1016/j.gca.2003.08.001.
- Lawrence, D. J., W. C. Feldman, B. L. Barraclough, A. B. Binder, R. C. Elphic, S. Maurice, and D. R. Thomsen (1998), Global elemental maps of the Moon: The lunar prospector gamma-ray spectrometer, *Science*, *281*, 1484, doi:10.1126/science.281.5382.148.
- Lawrence, D. J., W. C. Feldman, R. C. Elphic, R. C. Little, T. H. Prettyman, S. Maurice, P. G. Lucey, and A. B. Binder (2002), Iron abundances on the lunar surface as measured by the lunar prospector gamma-ray and neutron spectrometers, *J. Geophys. Res.*, *107*(E12), 5130, doi:10.1029/2001je001530.
- Le Mouélic, S., P. G. Lucey, Y. Langevin, and B. R. Hawke (2002), Calculating iron contents of lunar highland materials surrounding Tycho crater from integrated Clementine UV-visible and near-infrared data, *J. Geophys. Res.*, *107*(E10), 5074, doi:10.1029/2000je001484.
- Lucey, P. G., D. T. Blewett, and B. R. Hawke (1998), Mapping the FeO and TiO₂ content of the lunar surface with multispectral imagery, *J. Geophys. Res.*, *103*, 3679–3699, doi:10.1029/97JE03019.
- Lucey, P. G., D. T. Blewett, and B. L. Jolliff (2000a), Lunar iron and titanium abundance algorithms based on final processing of Clementine ultraviolet-visible images, *J. Geophys. Res.*, *105*(E8), 20297–20305, doi:10.1029/1999JE001117.
- Lucey, P. G., D. T. Blewett, G. J. Taylor, and B. R. Hawke (2000b), Imaging of lunar surface maturity, *J. Geophys. Res.*, *105*(E8), 20377–20386, doi:10.1029/1999JE001110.
- Lundeen, S., S. McLaughlin, and R. Alanis (2011), Moon Mineralogy Mapper data product software interface specification, NASA Planetary Data System.
- Malaret, E., P. Guasqui, S. McLaughlin, J. Sunshine, S. Besse, R. Clark, and P. Isaacson (2011), Ch1-Orb Moon M3 4 L2 reflectance near-IR spectral images V1.0, Ch1-Orb-L-M3-4-L2-Reflectance-V1.0, NASA Planetary Data System.
- McCord, T. B., R. N. Clark, B. R. Hawke, L. A. McFadden, P. D. Owensby, C. M. Pieters, and J. B. Adams (1981), Moon—Near-infrared spectral reflectance, a first good look, *J. Geophys. Res.*, *86*, 10883–10892, doi:10.1029/JB086iB11p10883.
- McEwen, A., E. Eliason, P. Lucey, E. Malaret, C. Pieters, M. Robinson, and T. Sucharski (1998), Summary of radiometric calibration and photometric normalization steps for the Clementine UVVIS images, *Lunar Planet. Sci.*, *29*, 1466.
- Morris, R. V. (1976), Surface exposure indices of lunar soils—A comparative FMR study, *Proc. Lunar Planet. Sci.*, *7*, 315–335.
- Morris, R. V. (1978), The surface exposure /maturity/ of lunar soils—Some concepts and I₀/FeO compilation, *Proc. Lunar Planet. Sci.*, *9*, 2287–2297.
- Mouroulis, P., R. G. Sellar, D. W. Wilson, J. J. Shea, and R. O. Green (2007), Optical design of a compact imaging spectrometer for planetary mineralogy, *Opt. Eng.*, *46*(063001), doi:10.1117/1.2749499.
- Mustard, J. F., and C. M. Pieters (1987), Quantitative abundance estimates from bidirectional reflectance measurements, *J. Geophys. Res.*, *92*, E617–E626, doi:10.1029/JB092iB04p0E617.
- Noble, S. K., C. M. Pieters, L. A. Taylor, R. V. Morris, C. C. Allen, D. S. McKay, and L. P. Keller (2001), The optical properties of the finest fraction of lunar soil: Implications for space weathering, *Meteorit. Planet. Sci.*, *36*, 31–42, doi:10.1111/j.1945-5100.2001.tb01808.x.
- Ohtake, M., et al. (2010), Deriving the absolute reflectance of lunar surface using SELENE (Kaguya) Multiband Imager Data, *Space Sci. Rev.*, *154*(1), 57–77, doi:10.1007/s11214-010-9689-0.
- Pieters, C. M. (1978), Mare basalt types on the front side of the Moon—A summary of spectral reflectance data, *Proc. Lunar Planet. Sci.*, *9*, 2825–2849.
- Pieters, C. M. (1986), Composition of the lunar highland crust from near-infrared spectroscopy, *Rev. Geophys. Sp. Phys.*, *24*(3), 557–578, doi:10.1029/RG024i003p00557.
- Pieters, C. M. (1999), The Moon as a spectral calibration standard enabled by lunar samples: The Clementine example, *Workshop on New Views of the Moon II: Understanding the Moon Through the Integration of Diverse Data sets*, 8025.
- Pieters, C. M., B. R. Hawke, M. Gaffey, and L. A. McFadden (1983), Possible lunar source areas of meteorite ALHA 81005 geochemical remote sensing information, *Geophys. Res. Lett.*, *10*, 813–816, doi:10.1029/GL010i009p00813.
- Pieters, C. M., E. M. Fischer, O. Rode, and A. Basu (1993), Optical effects of space weathering: The role of the finest fraction, *J. Geophys. Res.*, *98*, 20817–20824, doi:10.1029/93JE02467.
- Pieters, C. M., L. A. Taylor, S. K. Noble, L. P. Keller, B. Hapke, R. V. Morris, C. C. Allen, D. S. McKay, and S. Wentworth (2000), Space weathering on airless bodies: Resolving a mystery with lunar samples, *Meteorit. Planet. Sci.*, *35*, 1101–1107, doi:10.1111/j.1945-5100.2000.tb01496.x.
- Pieters, C. M., et al. (2009), The Moon Mineralogy Mapper (M³) on Chandrayaan-1, *Curr. Sci. India*, *96*(4), 500–505.
- Pieters, C. M., et al. (2011), Mg-spinel lithology: A new rock-type on the lunar farside, *J. Geophys. Res.*, *116*(E00G08), doi:10.1029/2010JE003727.
- Poulet, F., and S. Erard (2004), Nonlinear spectral mixing: Quantitative analysis of laboratory mineral mixtures, *J. Geophys. Res. (Planets)*, *109*, E02009, doi:10.1029/2003JE002179.
- Rodriguez, J. I., H. Tseng, and B. Zhang (2009), Thermal control system of the Moon Mineralogy Mapper instrument, *SAE Int. J. Aerosp.*, *1*(1), 376–387, doi:10.4271/2008-01-2119.
- Shkuratov, Y. G., V. G. Kaydash, C. Pieters, and N. V. Opanasenko (2000), A comparison of absolute calibrations of Clementine-UVVIS and Earth-based data for the Moon, *Lunar Planet. Sci.*, *31*, 1165.
- Staid, M. I., and C. M. Pieters (2000), Integrated spectral analysis of mare soils and craters: Applications to eastern nearside basalts, *Icarus*, *145*, 122–139, doi:10.1006/icar.1999.6319.
- Staid, M. I., et al. (2011), The mineralogy of late-stage lunar volcanism as observed by the Moon Mineralogy Mapper on Chandrayaan-1, *J. Geophys. Res.*, *116*(E00G10), doi:10.1029/2010JE003735.
- Sunshine, J. M., and C. M. Pieters (1998), Determining the composition of olivine from reflectance spectroscopy, *J. Geophys. Res.*, *103*, 13675–13688, doi:10.1029/98JE01217.
- Sunshine, J. M., C. M. Pieters, and S. F. Pratt (1990), Deconvolution of mineral absorption bands: An improved approach, *J. Geophys. Res.*, *95*(B5), 6955–6966, doi:10.1029/JB095iB05p06955.
- Taylor, L. A., C. M. Pieters, L. P. Keller, R. V. Morris, and D. S. McKay (2001), Lunar mare soils: Space weathering and the major effects of surface-correlated nanophase Fe, *J. Geophys. Res.*, *106*, 27985–28000, doi:10.1029/2000JE001402.
- Taylor, L. A., C. Pieters, A. Patchen, D.-H. S. Taylor, R. V. Morris, L. P. Keller, and D. S. McKay (2010), Mineralogical and chemical characterization of lunar highland soils: Insights into the space weathering of soils on airless bodies, *J. Geophys. Res.*, *115*, E02002, doi:10.1029/2009je003427.
- Tompkins, S., and C. M. Pieters (1999), Mineralogy of the lunar crust: Results from Clementine, *Meteorit. Planet. Sci.*, *34*(1), 25–41, doi:10.1111/j.1945-5100.1999.tb01729.x.